LETTER

doi:10.1038/nature24640

Mild oxidation of methane to methanol or acetic acid on supported isolated rhodium catalysts

Junjun Shan[1]*†, Mengwei Li[1]*, Lawrence F. Allard[2], Sungsik Lee[3] & Maria Flytzani-Stephanopoulos[1]

An efficient and direct method of catalytic conversion of methane to liquid methanol and other oxygenates would be of considerable practical value. However, it remains an unsolved problem in catalysis, as typically it involves expensive[1–4] or corrosive oxidants or reaction media[5–8] that are not amenable to commercialization. Although methane can be directly converted to methanol using molecular oxygen under mild conditions in the gas phase, the process is either stoichiometric (and therefore requires a water extraction step)[9–15] or is too slow and low-yielding[16] to be practical. Methane could, in principle, also be transformed through direct oxidative carbonylation to acetic acid, which is commercially obtained through methane steam reforming, methanol synthesis, and subsequent methanol carbonylation on homogeneous catalysts[17,18]. However, an effective catalyst for the direct carbonylation of methane to acetic acid, which might enable the economical small-scale utilization of natural gas that is currently flared or stranded, has not yet been reported. Here we show that mononuclear rhodium species, anchored on a zeolite or titanium dioxide support suspended in aqueous solution, catalyse the direct conversion of methane to methanol and acetic acid, using oxygen and carbon monoxide under mild conditions. We find that the two products form through independent pathways, which allows us to tune the conversion: three-hour-long batch-reactor tests conducted at 150 degrees Celsius, using either the zeolite-supported or the titanium-dioxide-supported catalyst, yield around 22,000 micromoles of acetic acid per gram of catalyst, or around 230 micromoles of methanol per gram of catalyst, respectively, with selectivities of 60–100 per cent. We anticipate that these unusually high activities, despite still being too low for commercial application, may guide the development of optimized catalysts and practical processes for the direct conversion of methane to methanol, acetic acid and other useful chemicals.

We prepared supported rhodium catalysts using relatively simple procedures. The main effort was to atomically disperse the rhodium species, which was achieved using a heat treatment protocol on the zeolite (ZSM-5) supports, and by anchoring rhodium precursor species on reduced titanium dioxide (titania) assisted by ultraviolet irradiation (see Methods). Rhodium loadings of 0.5 wt% and 0.6 wt% were used on the ZSM-5 and titanium dioxide supports, respectively.

The catalysts were suspended in water and tested in a batch reactor under a total pressure of CH_4, CO, and O_2 of less than 30 bar. The reactions were immediately activated and catalytic, as measured by catalyst turnover (Fig. 1). The light-off temperature—the temperature at which the catalytic reaction was initiated—was approximately 110 °C in the case of Rh-ZSM-5. When the temperature was increased from 130 °C to 150 °C the yield of liquid oxygenate increased substantially, although it decreased above 170 °C owing to over-oxidation to CO_2. Low temperatures and low partial pressure of oxygen (p_{O_2}) are desirable to suppress the over-oxidation. Figure 1a shows the effect of p_{O_2} on the formation of liquid oxygenates. The suppression of formic acid and CO_2 formation is notable upon decreasing p_{O_2} from 4 bar to 2 bar, and the selectivities for methanol and acetic acid increase appreciably. The selectivity is even higher at longer times (6 h) at a p_{O_2} of 2 bar (Fig. 1b). Under these conditions, the yield of acetic acid exceeds 13,000 μmol g_{cat}^{-1}, with approximately 60% selectivity. With increasing reaction time, the yield of acetic acid increases continuously while maintaining high selectivity, clearly showing that acetic acid is much less prone to over-oxidation than are formic acid or methanol. The calculated conversion of methane at $t = 6$ h is about 4% (Extended Data Table 1). The highest acetic acid selectivity was achieved with a p_{O_2} of 0.5 bar; however, the yield was rather low, indicating an oxygen-limited operation. By optimizing the preparation method of the Rh-ZSM-5 catalyst (see Methods), the yield of acetic acid can reach approximately 22,000 μmol g_{cat}^{-1} at $t = 3$ h (Fig. 1c).

The acidity of the zeolite has been reported to promote the selectivity of Cu-ZSM-5 catalysts for acetic acid[12]. To suppress the formation of acetic acid and tune the catalyst selectivity towards methanol, we used Na-ZSM-5. As shown in Fig. 1d, Rh–Na-ZSM-5 can selectively convert methane to methanol, and adding Cu^{2+} to the solution can further suppress the formation of formic acid (the role of Cu is discussed in the Methods). Although CO is not a reactant in the conversion of methane to methanol, its presence was found to be necessary for the catalyst to function. Methanol was also the exclusive product on rhodium/titanium dioxide catalysts, which lack the acidity of H-ZSM-5. The importance of this finding is twofold: it demonstrates that modulating the acidity of the support can be used to tune the formation of the desired product (acetic acid or methanol), and also shows that the confinement effect of the zeolite is not relevant in these reactions—an important result that could allow for a variety of oxide supports.

These findings were subject to further mechanistic investigation. First, analysis of the liquid after 12 h of reaction found only a trace amount of rhodium present, which we attributed to dissolution of the few rhodium nanoparticles present on the external surface of the zeolite (see Methods). However, methane conversion did not proceed further in solution after filtering out the catalyst. Therefore, the reaction is clearly heterogeneous. The state of the active rhodium species was also explored. Figure 2a and b show aberration-corrected high-angle annular dark-field scanning transmission electron microscopy (ac-HAADF/STEM) images of as-synthesized 0.5 wt% Rh-ZSM-5. Here, and as illustrated in further detail in Extended Data Fig. 2, contrast points consistent with the imaging of single rhodium atoms are found (circled). At lower magnification, part of the rhodium was found as nanoparticles on the external surfaces of the zeolite (Extended Data Fig. 3a–f). After sputtering the top surface layer of the zeolite particles, X-ray photoelectron spectroscopy (XPS) confirms the presence of rhodium species inside the zeolite micropores (Extended Data Fig. 3g and h).

[1]Department of Chemical and Biological Engineering, Tufts University, Medford, Massachusetts 02155, USA. [2]Materials Science and Technology Division, Oak Ridge National Laboratory, Oak Ridge, Tennessee 37831, USA. [3]X-ray Science Division, Argonne National Laboratory, 9700 South Cass Avenue, Argonne, Illinois 60439, USA. †Present address: NICE America Research, Inc., Mountain View, California 94043, USA.
*These authors contributed equally to this work.

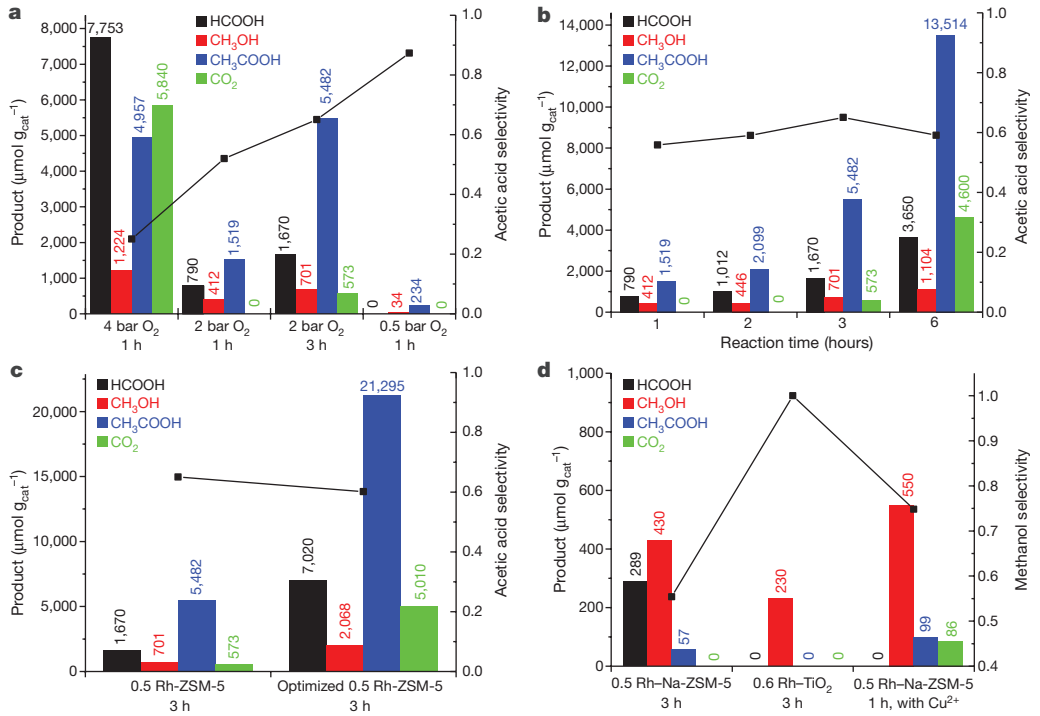

Figure 1 | Catalytic performance of supported rhodium catalysts in the conversion of methane to oxygenates. Reaction conditions: 20 mg catalyst, 0.5–4 bar O_2, 5 bar CO, 20 bar CH_4, 20 ml water, 0.5–6 h reaction time, 150 °C reaction temperature. **a**–**c**, Product yields and acetic acid selectivity for 0.5 wt% Rh-ZSM-5 with varying p_{O_2} and reaction time (**a**); 0.5 wt% Rh-ZSM-5 at 2 bar O_2 with varying reaction time (**b**); 0.5 wt% Rh-ZSM-5 and optimized 0.5 wt% Rh-ZSM-5 at 2 bar O_2 and 3 h reaction time (**c**). **d**, Product yields and methanol selectivity for 0.5 wt% Rh–Na-ZSM-5 with and without Cu^{2+}, as well as on 0.6 wt% rhodium/titanium dioxide, at 2 bar O_2 and varying reaction time.

Diffuse reflectance infrared Fourier transform spectroscopy using CO as a probe molecule (CO-DRIFTS) was performed on various active Rh-ZSM-5 catalysts under ambient conditions, as shown in Fig. 2c and d. Dicarbonyl species are formed on isolated rhodium cations, whereas on rhodium nanoparticles CO binds in both atop and bridged configurations[19]. The absorption peaks at 2,116 cm^{-1} and 2,049 cm^{-1} are attributed to the symmetrical and asymmetrical stretching of CO from the isolated mononuclear $Rh^{I}(CO)_2$ species[19], whereas the peak at 2,082 cm^{-1} is attributed to either the atop binding of CO on rhodium nanoparticles or isolated $Rh^{I}(CO)_3$ species[19,20]. The broad peak centred at 1,885 cm^{-1} is assigned to bridged CO on rhodium nanoparticles[19]. Applying a recently reported titration method[19], we estimated the portion of isolated rhodium to be 50%. Moreover, for 0.5 wt% Rh-ZSM-5_{washed} (see Methods), the peaks at 2,082 cm^{-1} and 1,885 cm^{-1} were difficult to see, indicating the dominance of isolated mononuclear $Rh^{I}(CO)_2$ species. As shown in Extended Data Fig. 4a, the selectivities of the parent 0.5 wt% Rh-ZSM-5 and the 0.5 wt% Rh-ZSM-5_{washed} samples are similar, and their activities were also comparable, indicating that they possess the same active sites. Similar spectra were also obtained for the optimized Rh-ZSM-5 catalyst, comprising isolated rhodium cations. Hence, the optimized Rh-ZSM-5 catalyst shows superior catalytic activity because of the greater number of isolated rhodium species inside the micropores (Fig. 1c).

Figure 2d shows CO-DRIFTS spectra of Rh-ZSM-5 upon H_2 and static air treatment. For the latter, the $Rh^{I}(CO)_2$ peaks are absent and a single broad peak centred at 2,045 cm^{-1} appears, which is assigned to atop binding of CO on rhodium/rhodium oxide nanoparticles[21]. This finding is corroborated by ultraviolet–visible (UV–Vis) absorption spectroscopic characterization of the O_2- and H_2-treated samples (Extended Data Fig. 5a). It is suggested that the heat treatment during the preparation step controls the type of rhodium sites. It has been reported that H_2 heat treatment of Fe-ZSM-5 during the preparation step favours the formation of isolated iron cations[22]. Similarly, isolated Rh^{+} cations were obtained here by reducing the precursors in H_2. By contrast, static air calcination favours the formation of rhodium oxide nanoparticles. Extended Data Fig. 4a also shows that Rh-ZSM-5 reduced in H_2 is much more active than Rh-ZSM-5 calcined in air. Furthermore, no activity was found on silica-supported rhodium or rhodium oxide nanoparticles. We therefore conclude that the active sites are the isolated mononuclear rhodium species inside the zeolite micropores.

Linear combination fitting of X-ray absorption near edge structure (XANES) data of 0.5 wt% Rh-ZSM-5_{washed} shows that rhodium is mostly in the +1 oxidation state (Extended Data Fig. 5b), whereas 0.5 wt% Rh-ZSM-5 (without washing) consists of 60% Rh^{+} and 40% metallic rhodium, which is comparable to the amount estimated from DRIFTS. Extended Data Fig. 6 shows extended X-ray absorption fine structure (EXAFS) data of 0.5 wt% Rh-ZSM-5_{washed}, and the quantitative analysis reveals that there is no distinct Rh–Rh bonding (Extended Data Table 2). XANES and EXAFS data were also collected for the same catalysts suspended in water, to mimic the reaction conditions, and no noticeable difference was found. Therefore, these measurements also support the single-site distribution of isolated Rh^{+} cations.

It has been reported that C–H bond activation can proceed over an isolated transition-metal centre, yielding M–CH_3 species[23]. Here, we hypothesize that isolated Rh^{+} cations facilitate the activation of methane in water by O_2 to form Rh–CH_3 species, which can be further functionalized under our reaction conditions. This hypothesis is supported by our catalysis measurements. As shown in entries 2 and 3 of Table 1, when using only CH_4 with CO or only CH_4 with O_2, no oxygenates were formed. In entry 4, after exposure to CH_4 and O_2 at 150 °C for 1 h, the reactor was cooled to less than 10 °C and purged with He several times, then 5 bar CO was added and the catalyst was heated to 150 °C for 1 h. In this case, 23 μmol g_{cat}^{-1} of acetic acid was formed.

Methane can therefore be activated by O_2 to form Rh–CH_3 species, which can be further functionalized by CO to produce acetic acid. Assuming a 1:1 stoichiometric ratio of rhodium to methyl group, this corresponds to ~23 μmol g_{cat}^{-1} Rh–CH_3. On the basis of DRIFTS and

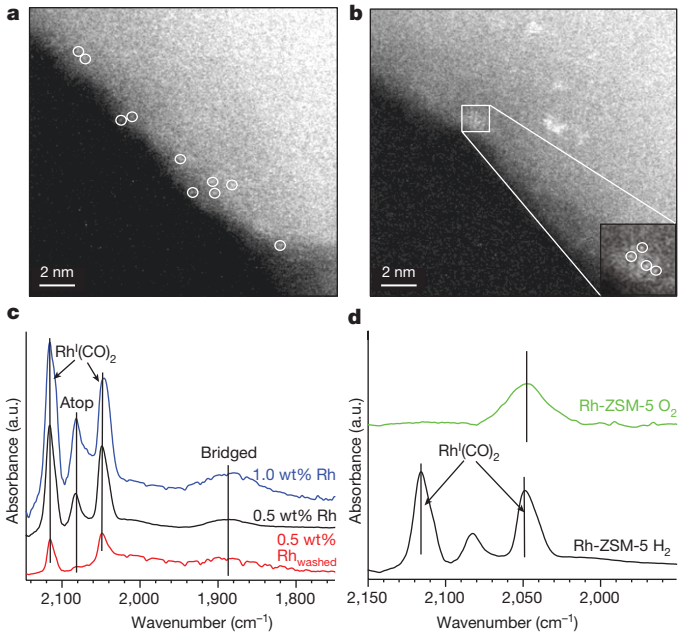

Figure 2 | TEM images and CO-DRIFTS spectra of various Rh-ZSM-5 catalysts. a, **b**, ac-HAADF-STEM images of a thin edge of an as-synthesized Rh-ZSM-5 flake. Isolated rhodium atoms are marked with white circles. **c**, CO-DRIFTS spectra of 1.0 wt% Rh-ZSM-5, 0.5 wt% Rh-ZSM-5 and 0.5 wt% Rh-ZSM-5$_{washed}$; an additional washing step was applied to the latter sample before the hydrogen reduction step to remove rhodium species from the external surface of the zeolite; **d**, CO-DRIFTS spectra of 0.5 wt% Rh-ZSM-5 (bottom trace) and 0.5 wt% Rh-ZSM-5 calcined in air (top trace). See Methods for further details.

XANES measurements, for as-synthesized 0.5 wt% Rh-ZSM-5, about 25 μmol g_{cat}^{-1} (approximately 55%) of Rh is present as isolated cations, which agrees well with the formation of about 23 μmol g_{cat}^{-1} Rh–CH_3. By contrast, the formation of 4,957 μmol g_{cat}^{-1} of acetic acid (entry 5 of Table 1) shows that, when all three gases are present, the reaction is not stoichiometric, but clearly catalytic with a closed cycle.

According to various reports[8,24,25], CO may insert directly into Rh–CH_3 bonds through carbonylation insertion to form Rh–$COCH_3$ species, which can be further hydrolysed to acetic acid in water. As discussed in Methods, isotope labelling measurements with ^{13}CO were used to confirm its insertion. However, our measurements also show that such insertion requires acidity of the zeolite support. As shown in Fig. 1d, when using Rh–Na-ZSM-5 the yield of acetic acid was greatly reduced compared with that obtained using Rh-ZSM-5; the former contains far fewer Brønsted acid sites[12]. Similar observations were made for the rhodium/titanium dioxide sample (Fig. 1d); there is no formation of acetic acid in this case. The Brønsted acid sites of the zeolite are therefore necessary for the formation of acetic acid.

To determine whether methanol is a reaction intermediate in the formation of acetic acid, we also performed catalytic tests using methanol, CO and O_2 as the reactants. 1 mM methanol in 20 ml water, 5 bar CO, 4 bar O_2 and 20 mg 0.5 wt% Rh-ZSM-5 were heated to 150 °C for 1 h. No formation of acetic acid or formic acid was observed, indicating that methanol is not a reaction intermediate in the conversion of methane to acetic acid or formic acid. Instead, methanol and acetic acid are produced through independent reaction pathways (Extended Data Fig. 7).

Moreover, entry 4 in Table 1 also shows that only acetic acid was formed when CO was used to sweep the catalyst after the formation of Rh–CH_3. Therefore, methanol and formic acid must be produced by a different reaction pathway. Using density functional theory calculations, it has been shown previously that an oxygen atom can insert into the M–CH_3 bond in the presence of a CO ligand to form M–OCH_3,

Table 1 | Liquid oxygenates produced on bare ZSM-5 and as-synthesized 0.5 wt% Rh-ZSM-5

Catalyst*	Conditions**	Product (μmol g_{cat}^{-1})		
		CH_3OH	HCOOH	CH_3COOH
ZSM-5	CH_4+O_2+CO, 150 °C, 1 h	0	0	0
0.5 wt% Rh-ZSM-5	CH_4+CO, 150 °C, 1 h	0	0	0
0.5 wt% Rh-ZSM-5	CH_4+O_2, 150 °C, 1 h	0	0	0
0.5 wt% Rh-ZSM-5	CH_4+O_2, 150 °C, 1 h; purge, addition of CO, 150 °C, 1 h	0	0	23
0.5 wt% Rh-ZSM-5	CH_4+O_2+CO, 150 °C, 1 h	1,224	7,753	4,957

*After impregnation, all samples were vacuum dried at 60 °C, followed by reduction in 5% H_2 at 550 °C for 3 h at a heating rate of 3 °C min^{-1}.
**In all tests, the same partial pressures (in bar) of the reactants were used: CH_4, 20; CO, 5; O_2, 4. 20 mg catalyst suspended in 20 ml water was used.

which can be further hydrolysed to methanol[26]. Similarly, our experiments suggest that Rh–CH_3 can form Rh–OCH_3 species by the insertion of an oxygen atom in the presence of CO ligands that bind with rhodium. The formed Rh–OCH_3 will be hydrolysed to produce methanol. Furthermore, isotope-labelling measurements with ^{13}CO confirm that the methyl-group carbon is derived solely from methane, not from carbon monoxide, suggesting that CO is acting as a co-catalyst. It has been reported that, in the catalytic oxidation of methane to methanol with hydrogen peroxide, a reductant is required to regenerate the copper catalyst[3]. It is likely that CO can also regenerate Rh-ZSM-5 catalysts to preserve the Rh^+ active sites. In addition, Fig. 1d indicates that, for the formation of methanol, acidity of the zeolite support is not required.

The conversion of methane to oxygenates may therefore occur via a two-step reaction pathway: methane activation followed by M–CH_3 functionalization (Extended Data Fig. 7). In the first step, methane is activated in the presence of O_2 on isolated Rh^+ cations under mild conditions to produce Rh–CH_3. The exact mechanism responsible for this activation is not clear and warrants further investigation. The formed Rh–CH_3 can then be functionalized via two independent reaction pathways: oxygen insertion to produce methanol, or CO insertion to produce acetic acid. After the hydrolysis step, isolated Rh^+ species are available for the next catalytic cycle.

Further investigation of the Rh–CH_3 functionalization step, for which CO is required, is necessary to guide the design of new and more efficient methane oxidation catalysts and processes, especially for direct methane-to-methanol conversion. More immediate practical value may be offered by the acetic acid production pathway, as dilute solutions of acetic acid could serve as nutrient streams to microbes, which can convert and sequester them into highly concentrated lipid products[27].

Online Content Methods, along with any additional Extended Data display items and Source Data, are available in the online version of the paper; references unique to these sections appear only in the online paper.

Received 18 August 2016; accepted 2 October 2017.

1. Hammond, C. *et al.* Direct catalytic conversion of methane to methanol in an aqueous medium by using copper-promoted Fe-ZSM-5. *Angew. Chem. Int. Ed. Engl.* **51,** 5129–5133 (2012).
2. Hammond, C. *et al.* Elucidation and evolution of the active component within Cu/Fe/ZSM-5 for catalytic methane oxidation: from synthesis to catalysis. *ACS Catal.* **3,** 689–699 (2013).
3. Liu, C. C., Mou, C. Y., Yu, S. S. F. & Chan, S. I. Heterogeneous formulation of the tricopper complex for efficient catalytic conversion of methane into methanol at ambient temperature and pressure. *Energy Environ. Sci.* **9,** 1361–1374 (2016).
4. McFarland, E. Unconventional chemistry for unconventional natural gas. *Science* **338,** 340–342 (2012).
5. Gol'dshleger, N. F., Tyabin, M. B., Shilov, A. E. & Shteinman, A. A. Activation of saturated hydrocarbons. Deuterium-hydrogen exchange in solutions of transition metal complexes. *Russ. J. Phys. Chem. A.* **43,** 1222–1223 (1969).
6. Periana, R. A. *et al.* Platinum catalysts for the high-yield oxidation of methane to a methanol derivative. *Science* **280,** 560–564 (1998).

7. Chepaikin, E. G. *et al.* Functionalisation of methane under dioxygen and carbon monoxide catalyzed by rhodium complexes: oxidation and oxidative carbonylation. *J. Mol. Catal. Chem.* **169,** 89–98 (2001).
8. Periana, R. A., Mironov, O., Taube, D., Bhalla, G. & Jones, C. J. Catalytic, oxidative condensation of CH_4 to CH_3COOH in one step via CH activation. *Science* **301,** 814–818 (2003).
9. Groothaert, M. H., Smeets, P. J., Sels, B. F., Jacobs, P. A. & Schoonheydt, R. A. Selective oxidation of methane by the bis(μ-oxo)dicopper core stabilized on ZSM-5 and mordenite zeolites. *J. Am. Chem. Soc.* **127,** 1394–1395 (2005).
10. Sushkevich, V. L., Palagin, D., Ranocchiari, M. & van Bokhoven, J. A. Selective anaerobic oxidation of methane enables direct synthesis of methanol. *Science* **356,** 523–527 (2017).
11. Grundner, S. *et al.* Single-site trinuclear copper oxygen clusters in mordenite for selective conversion of methane to methanol. *Nat. Commun.* **6,** 7546 (2015).
12. Narsimhan, K. *et al.* Methane to acetic acid over Cu-exchanged zeolites: mechanistic insights from a site-specific carbonylation reaction. *J. Am. Chem. Soc.* **137,** 1825–1832 (2015).
13. Starokon, E. V., Parfenov, M. V., Pirutko, L. V., Abornev, S. I. & Panov, G. I. Room-temperature oxidation of methane by α-oxygen and extraction of products from the FeZSM-5 surface. *J. Phys. Chem. C* **115,** 2155–2161 (2011).
14. Beznis, N. V., van Laak, A. N. C., Weckhuysen, B. M. & Bitter, J. H. Oxidation of methane to methanol and formaldehyde over Co-ZSM-5 molecular sieves: tuning the reactivity and selectivity by alkaline and acid treatments of the zeolite ZSM-5 agglomerates. *Micropor. Mesopor. Mater.* **138,** 176–183 (2011).
15. Shan, J. *et al.* Conversion of methane to methanol with a bent mono(μ-oxo) dinickel anchored on the internal surfaces of micropores. *Langmuir* **30,** 8558–8569 (2014).
16. Narsimhan, K., Iyoki, K., Dinh, K. & Román-Leshkov, Y. Catalytic oxidation of methane into methanol over copper-exchanged zeolites with oxygen at low temperature. *ACS Cent. Sci.* **2,** 424–429 (2016).
17. Paulik, F. E. & Roth, J. F. Novel catalysts for the low-pressure carbonylation of methanol to acetic acid. *Chem. Commun.* 1578a (1968).
18. Lin, M. & Sen, A. Direct catalytic conversion of methane to acetic acid in an aqueous medium. *Nature* **368,** 613–615 (1994).
19. Matsubu, J. C., Yang, V. N. & Christopher, P. Isolated metal active site concentration and stability control catalytic CO_2 reduction selectivity. *J. Am. Chem. Soc.* **137,** 3076–3084 (2015).
20. Ivanova, E. & Hadjiivanov, K. Polycarbonyls of Rh^+ formed after interaction of CO with Rh–MFI: an FTIR spectroscopic study. *Phys. Chem. Chem. Phys.* **5,** 655–661 (2003).
21. Kroner, A. B. *et al.* Time-resolved, *in situ* DRIFTS/EDE/MS studies on alumina-supported rhodium catalysts: effects of ceriation and zirconiation on rhodium–CO interactions. *ChemPhysChem* **15,** 3049–3059 (2014).
22. Forde, M. M. *et al.* Light alkane oxidation using catalysts prepared by chemical vapour impregnation: tuning alcohol selectivity through catalyst pre-treatment. *Chem. Sci.* **5,** 3603–3616 (2014).
23. Olivos-Suarez, A. I. *et al.* Strategies for the direct catalytic valorization of methane using heterogeneous catalysis: challenges and opportunities. *ACS Catal.* **6,** 2965–2981 (2016).
24. Wang, X. *et al.* NMR-spectroscopic evidence of intermediate-dependent pathways for acetic acid formation from methane and carbon monoxide over a ZnZSM-5 zeolite catalyst. *Angew. Chem. Int. Ed.* **51,** 3850–3853 (2012).
25. Cavell, K. J. Recent fundamental studies on migratory insertion into metal-carbon bonds. *Coord. Chem. Rev.* **155,** 209–243 (1996).
26. Pardue, D. B., Mei, J., Cundari, T. R. & Gunnoe, T. B. Density functional theory study of oxygen-atom insertion into metal–methyl bonds of iron(II), ruthenium(II), and osmium(II) complexes: study of metal-mediated C–O bond formation. *Inorg. Chem.* **53,** 2968–2975 (2014).
27. Xu, J., Liu, N., Qiao, K., Vogg, S. & Stephanopoulos, G. Application of metabolic controls for the maximization of lipid production in semicontinuous fermentation. *Proc. Natl Acad. Sci. USA* **114,** E5308–E5316 (2017).

Acknowledgements The financial support of this work by the Department of Energy, DOE/ARPA-e grant DE-AR0000433, under subcontract from MIT, is gratefully acknowledged. The XAS work used resources of the Advanced Photon Source, a US Department of Energy (DOE) Office of Science, User Facility operated for the DOE Office of Science by Argonne National Laboratory under contract DE-AC02-06CH11357. Aberration-corrected electron microscopy research at Oak Ridge National Laboratory was sponsored by the US Department of Energy, Office of Energy Efficiency and Renewable Energy, Vehicle Technologies Office, Propulsion Materials Program.

Author Contributions J.S. conceived the research, designed the experiments, characterized the samples and drafted the manuscript. M.L. conceived the research and performed catalytic evaluation. M.F.-S. conceived the research and designed the experiments. L.F.A was responsible for the STEM characterization. S.L. helped with the XANES and EXAFS measurements and the interpretation of the results. All the authors discussed the results and participated in writing the manuscript.

Author Information Reprints and permissions information is available at www.nature.com/reprints. The authors declare no competing financial interests. Readers are welcome to comment on the online version of the paper. Publisher's note: Springer Nature remains neutral with regard to jurisdictional claims in published maps and institutional affiliations. Correspondence and requests for materials should be addressed to M.F.-S. (maria.flytzani-stephanopoulos@tufts.edu).

Reviewer Information *Nature* thanks E. Pidko and the other anonymous reviewer(s) for their contribution to the peer review of this work.

METHODS

Catalyst preparation. The Rh-ZSM-5 catalysts were prepared in several steps. First, the ammonium form of the zeolite, NH_4-ZSM-5, with Si:Al ratios of 15 and 100, purchased from Alfa, was used without further modification. Preliminary catalysis tests found that catalysts synthesized from ZSM-5 with a Si:Al ratio of 15 were more active than those synthesized from ZSM-5 with a Si:Al ratio of 100. The former was adopted for use, therefore ZSM-5 herein refers to the zeolite with a Si:Al ratio of 15. Inductively coupled plasma elemental analysis showed that the concentrations of Cu and Fe in the purchased NH_4-ZSM-5 were 0 and 0.002 wt%, respectively. Such a low concentration of Fe impurities does not produce any detectable products under our reaction conditions. In the second step, residual water was removed from the internal pores of the zeolite by drying in a vacuum oven at 120 °C for 3 h. Rh precursors were then introduced by incipient wetness impregnation with a Rh(III) nitrate solution (99%, Sigma-Aldrich) into the dehydrated NH_4-ZSM-5. After impregnation, the samples were dried in a vacuum oven at 60 °C overnight, then reduced in 5% H_2 (balanced in helium) at 550 °C for 3 h at a heating rate of 3 °C min^{-1}, and subsequently labelled as 'as-synthesized Rh-ZSM-5'. For clarity, Rh-ZSM-5 here refers to the catalyst that was reduced in 5% H_2, unless otherwise noted. For comparison, part of the samples after drying in the vacuum oven were calcined in static air at 550 °C for 3 h instead of reducing in a hydrogen atmosphere; these are labelled as 'Rh-ZSM-5 O_2'. An additional washing and filtration step was applied to some samples before the reduction to remove the Rh species present at the pore mouths on the external surface of the zeolite; these are labelled as 'Rh-ZSM-5_{washed}'. In this washing and filtration step the zeolite was washed dropwise with deionized water, filtered and then dried in a vacuum oven at 60 °C overnight. Rh-ZSM-5 catalysts with different nominal Rh loadings were prepared. The concentrations of Rh were determined by inductively coupled plasma optical emission spectrometry (ICP–OES).

A large fraction of the rhodium is stabilized in single ion form by this preparation, with the remainder forming nanoparticles on the external surface of the zeolite. X-ray diffraction (XRD) patterns of as-synthesized 0.5 wt% Rh-ZSM-5, and of the same catalyst after use in the reaction, are shown in Extended Data Fig. 1. Neither the impregnation nor the reaction conditions caused any changes in the ZSM-5 crystal structure. Furthermore, we also used Mordenite zeolite (MOR) with a Si:Al ratio of 10, to prepare Rh–MOR by similar methods. The catalytic tests showed that Rh–MOR exhibits similar catalytic performance to the ZSM-5 based catalysts.

To prepare the optimized Rh-ZSM-5, an additional washing and filtration step was first applied to samples before the reduction to remove the Rh species present at the pore mouths on the external surface of the zeolite; the sample was then dried in a vacuum oven at 60 °C overnight. The same impregnation, washing, drying steps were then repeated four times, followed by reduction in 5% H_2 at 550 °C for 3 h to obtain the final catalytic material.

We also prepared several Rh-ZSM-5 catalysts by using Rh(III) chloride as a precursor instead of Rh(III) nitrate. The catalytic tests showed similar activity for the samples prepared with Rh(III) chloride as for those prepared with Rh(III) nitrate, indicating that the presence of the Cl in the impregnation step does not affect the activity of the catalysts following reduction in H_2 at 550 °C.

The sodium-ion-exchanged 0.5 wt% Rh-ZSM-5 catalyst was prepared by mixing 1 g of 0.5 wt% Rh-ZSM-5 in 36 ml of a 2.44 M solution of sodium acetate at 80 °C for 12 h. Samples were then filtered and washed with hot deionized water, followed by drying in a vacuum oven at room temperature overnight. This procedure was repeated twice to obtain the sodium-ion-exchanged Rh-ZSM-5 catalyst.

A commercial titanium oxide, TiO_2 (Millenium, G5, anatase) was used to prepare TiO_2-supported isolated Rh cation catalysts. The preparation involves first the deposition of Rh species onto TiO_2 via deposition–precipitation, using an aqueous solution of Rh(III) nitrate. The desired amount of Rh(III) nitrate solution was added dropwise into the TiO_2 suspension, which was maintained at a temperature of 80 °C and a pH of 8.5. The suspension was further held at 80 °C for 3 h, the solids were filtered and transferred to an ethanol solution, and then the slurry was exposed to ultraviolet irradiation with an 8 W black light lamp centred at 365 nm. During the irradiation process, Rh cations are anchored on certain surface sites of the titanium dioxide[28]. Excess Rh, weakly bound on the surface, can be readily removed by hydrochloric acid. Starting from 2.5 wt% Rh/TiO_2 using the deposition–precipitation method, ultraviolet irradiation for 3 h can anchor ~0.6 wt% Rh as single atoms on this support, on the basis of our characterization.

Catalyst characterization. After preparation, Rh-ZSM-5 catalysts were characterized by XRD, ac-HAADF/STEM, XPS, DRIFTS, UV–Vis absorption spectroscopy, XANES and EXAFS.

XRD patterns were collected on a PANalytical X'Pert Pro instrument using nickel-filtered Cu Kα radiation ($\lambda = 1.54056$ Å). The measurements were taken at 45 kV and 40 mA in a continuous mode and a 2θ range from 10° to 60°. XPS data were collected in a PHI VersaProbe II system equipped with a monochromatic Al Kα source and a double-focusing hemispherical analyser. The XPS system was also equipped with an argon ion sputtering gun to sputter the sample for depth-profile analysis. XPS samples were prepared by loading the catalyst powder onto a Cu foil. XPS data analysis was performed with CASA XPS software.

Ac-HAADF/STEM images of Rh-ZSM-5 were obtained with a JEOL 2200FS-AC (S)TEM instrument at Oak Ridge National Laboratory, fitted with a CEOS GmbH corrector on the probe-forming lenses and operating at 200 kV for all analyses. The samples for high-resolution imaging were prepared by dispersing the Rh-ZSM-5 powder in water and adding a few drops onto copper grids supported on carbon films. Energy-dispersive X-ray analysis data were obtained using a Bruker-AXS 30 mm^2 silicon-drift detector system. Trial imaging experiments allowed the determination of the most appropriate beam conditions to minimize loss of the zeolite crystal structure when scanning the sample for the best thin edges of powder support particles to examine. An incident probe with a nominal 14-pA current at a convergence semi-angle of 26.5° was used (mag mode 9C on the JEOL 2200FS instrument). In comparison, catalyst samples with more stable support materials are typically imaged with beam currents of 41 pA to achieve 0.07 nm resolution for single-atom imaging on stable supports. The large beam convergence semi-angle for HAADF imaging results in a focal depth of only a few nanometres, and atoms outside of a given focus point gradually reduce in contrast, so it was expected that the Rh atoms in the ZSM-5 material would be rather difficult to image, since they would probably be not only at different z-height positions in the lattice, but would also be affected by the simultaneous degradation of the cage structure of the zeolite while the electron beam was forming the scanned image. Any atom motion during imaging also degrades the contrast. Nevertheless, images were obtained as illustrated in Extended Data Fig. 2 (and Fig. 2a and b), which shows both the raw image and the processed image of a thin edge of a ZSM-5 flake, clearly amorphized by the incident beam, in which the eye can select contrast points in the raw image that are enhanced in the processed image.

DRIFTS measurements were conducted on a Thermo Scientific Nicolet iS50 FTIR spectrometer and a Praying Mantis high temperature reaction chamber. The CO adsorption on various samples was measured at room temperature. Pure CO was introduced into the DRIFTS cell at a flow rate of 10 ml min^{-1}. This was followed by a He purge at a flow rate of 20 ml min^{-1} to remove gas-phase CO from the cell before DRIFTS measurements. UV–Vis absorption spectra were collected in the range of 200–800 nm using a Jasco V570 UV–Vis spectrophotometer.

XANES and EXAFS data were obtained at beamline 12-BM at the Argonne National Laboratory. The data for Rh-ZSM-5 at the Rh K-edge in the fluorescence mode were collected at room temperature. To avoid the influence of Rh nanoparticles present on the external surface of the zeolite, the majority of Rh-ZSM-5 EXAFS samples were pre-washed with deionized water as described above. Approximately five consecutive scans were run for each sample to improve the signal-to-noise ratio. EXAFS data processing and analysis were performed using the IFEFFIT package.

Catalytic evaluation. Batch-reactor tests were conducted at a fixed methane pressure of 20 bar and a typical charge of 20 mg catalyst suspended in 20 ml water in a Parr reactor. The other two gases, O_2 and CO, were used at lower partial pressures, 0.5–5 bar, and the temperature was varied over the range of 100–170 °C. Liquid product analysis was performed using ^{1}H NMR, and gaseous samples were analysed by gas chromatography and mass spectrometry.

The catalytic tests were performed in a Parr high-pressure micro reactor (series 4590), which has a maximum working pressure of 1,000 psi, and a maximum working temperature of 350 °C. The maximum liquid volume is 35 ml. A magnetic stir bar was used to continuously stir the solution during the reaction, and an oil bath was used to heat the reactor. A K-type thermocouple was inserted into the Parr reactor to directly measure the temperature of the liquid.

During the reaction, a certain amount of catalyst was added into 20 ml deionized water followed by ultrasonic sonication for 1 min. The reactor vessel was pressurized using 0.5–4 bar O_2, 5 bar CO and 20 bar CH_4. The reactor was then placed in an oil bath that was pre-heated to the desired temperature, and the solution was heated to a certain temperature for a certain period of time under constant stirring. After the reaction, the reactor was removed from the oil bath and cooled with ice. Once the temperature of the reaction solution was below 10 °C, the gas composition was analysed by both gas chromatography and mass spectrometry to check for CO_2 formation, and the liquid was collected in a vial after filtering out the solid particles. It should be noted that CO_2 originates from two different reactions, namely the over-oxidation of liquid oxygenates and the direct conversion of CO to CO_2 through CO oxidation. The amount of CO_2 formed from CO was determined from a separate experiment using identical reaction conditions but without CH_4. The amount of CO_2 originating from CH_4 was then calculated by subtracting the CO_2 produced as a result of CO oxidation from the total amount of CO_2 formed.

The carbon balance, including all CH_4 and CO derived products, was over 97% for the catalytic tests conducted.

The concentration of oxygenates in the liquid was quantified by NMR. ^{1}H NMR spectra were measured on a Bruker AVANCE III 500 spectrometer. The measurement was calibrated using a 1% tetramethylsilane (TMS)/$CDCl_3$ internal standard. Typically, 0.6 ml liquid was mixed with 0.1 ml of D_2O to prepare a solution in an NMR sample tube for the measurement. The signal of protons from the solvent H_2O is much higher than that from the products. Therefore, all ^{1}H NMR spectra were recorded using a pre-saturation solvent suppression technique to suppress the dominant H_2O signal. The typical products—methanol, formic acid and acetic acid—were quantified by comparing the ^{1}H NMR signal against calibration curves for each molecule.

In this study, each single data point in conversion measurements was repeated at least three times under the same conditions. The uncertainties of these measurements were typically below 10%. The average value of these results is presented in the paper.

Extended results and discussion. Extended Data Fig. 1 shows XRD patterns of bare ZSM-5, as-synthesized 0.5 wt% Rh-ZSM-5, as well as 0.5 wt% Rh-ZSM-5 after 1 h and after 3 h of reaction at 150 °C. XRD patterns of as-synthesized Rh-ZSM-5 show no observable difference compared with bare ZSM-5, indicating that the impregnation of Rh does not change the lattice structure of ZSM-5. The XRD patterns of Rh-ZSM-5 catalysts after the 1 h and 3 h reaction tests are preserved, suggesting that the methane oxidative conversion reaction does not alter the lattice structure of ZSM-5. Previous studies of zeolite stability have reported that under hydrothermal conditions the framework of certain types of zeolites is prone to hydrolysis of the siloxane bond, which leads to the destruction of the framework, for example the HY zeolite[29]. However, the stability of zeolites under hydrothermal conditions is heavily affected by the type of framework. For example, zeolite Y becomes amorphous after treatment in water at 200 °C for 6 h, whereas the framework of ZSM-5 remains unmodified under the same conditions[30]. Similarly, based on XRD, under our reaction conditions the zeolite lattice structure of Rh-ZSM-5 catalyst does not change. In addition, Extended Data Fig. 1 also shows that no diffraction peaks related to Rh oxide or metallic nanoparticles are present[31], indicating well dispersed Rh species.

Extended Data Fig. 2 shows ac-HAADF/STEM images of a thin edge of the as-synthesized Rh-ZSM-5 flake, where it is possible to image the Rh atoms. Extended Data Fig. 2a is the raw HAADF/STEM image, and Extended Data Fig. 2b is the image after five-point smoothing and small contrast enhancement. Here, an incident probe with a nominal 14-pA current at a convergence semi-angle of 26.5° was used (that is, mag mode 9C on the JEOL 2200FS instrument). As shown in the images, contrast points consistent with the imaging of single Rh atoms are circled. Extended Data Fig. 3a–f show ac-HAADF and bright-field image pairs of various 0.5 wt% Rh-ZSM-5 catalysts at higher magnification. Extended Data Fig. 3a and b show the images of as-synthesized 0.5 wt% Rh-ZSM-5, whereas Extended Data Fig. 3c and d are the images of the 0.5 wt% Rh-ZSM-5 catalysts after use in the reaction, and Extended Data Fig. 3e and f show the images of 0.5 wt% Rh-ZSM-5_{washed}. These HAADF and bright-field image pairs were acquired simultaneously. TEM images clearly show that, for the samples without the additional washing step, there are a few Rh nanoparticles present on the external surface of the zeolite, whereas for Rh-ZSM-5_{washed} there are no Rh nanoparticles present on the external surface of the zeolite. This observation is consistent with the CO-DRIFTS findings (Fig. 2c).

Extended Data Fig. 3g and h show photoemission features of Rh 3*d* (Fig. 3g) and Si 2*p* (Fig. 3h) of as-synthesized 0.5 wt% Rh-ZSM-5 before and after Ar^+ sputtering. Extended Data Fig. 3g shows that, before sputtering, no photoemission peak of Rh was observed for the as-synthesized 0.5 wt% Rh-ZSM-5 sample. This means that the amount of Rh on the external surface of the zeolite is below the detection limit of XPS. To study the Rh species anchored on the internal walls of Rh-ZSM-5, the oxide surface layers of ZSM-5 must be removed[15]. After Ar^+ ion sputtering for 5 min, sufficient layers of silica on the external surface of Rh-ZSM-5 were removed, and the Rh 3*d* feature arising from the Rh species anchored on the internal walls of zeolite was clearly identified in Extended Data Fig. 3g[32]. Conversely, the photoemission feature of Si 2*p* (Extended Data Fig. 3h) shows no difference before and after Ar^+ ion sputtering.

Extended Data Fig. 4a shows the yields of liquid oxygenates on Rh-ZSM-5 catalysts with different Rh loadings, as well as 0.5 wt% Rh-ZSM-5_{washed} and 0.5 wt% Rh-ZSM-5 O_2. The data demonstrate that among the samples 0.1 wt% Rh-ZSM-5, 0.5 wt% Rh-ZSM-5, 1.0 wt% Rh-ZSM-5 and 0.5 wt% Rh-ZSM-5 O_2, 0.5 wt% Rh-ZSM-5 exhibits the best catalytic performance. Compared to 0.1 wt% Rh-ZSM-5, it is likely that 0.5 wt% Rh-ZSM-5 has more active sites, thereby explaining its superior activity. By contrast, 1.0 wt% Rh-ZSM-5 is inferior owing to the presence of rhodium particles, which may partially block access to the zeolite pores and decrease the activity. For Rh-ZSM-5 O_2, the presence of rhodium oxide nanoparticles suppresses the activity. Moreover, for 0.5 wt% Rh-ZSM-5_{washed}, ICP analysis shows that the residual Rh loading is ~0.13 wt%; that is, ~75% Rh species were removed by the additional washing step. Clearly, washing not only removes the Rh species on the external surface but also some Rh precursor species from the zeolite micropores, which will form isolated Rh cations after the reduction step. Therefore, the content of active sites in 0.5 wt% Rh-ZSM-5_{washed} is between 0.1 wt% Rh and 0.5 wt% Rh in the ZSM-5. The yields of oxygenates for 0.5 wt% Rh-ZSM-5_{washed} are also between these two values. In other words, the intrinsic catalytic activity of Rh-ZSM-5_{washed} per Rh atom is comparable to Rh-ZSM-5 without washing. If the washing step is performed after the reduction, the anchored Rh species cannot be removed by the mild washing step.

Extended Data Fig. 4b shows the product yields and selectivity to liquid oxygenates at various reaction times with $p_{O_2} = 4$ bar, using the as-synthesized 0.5 wt% Rh-ZSM-5 catalyst. At $t \leq 0.5$ h, the selectivity to liquid oxygenates is close to 90%, but the yield of acetic acid (1,976 μmol g_{cat}^{-1}) is lower than that of formic acid (9,263 μmol g_{cat}^{-1}); that is, 0.5 wt% Rh-ZSM-5 is more active for the oxidation of methane to formic acid under these conditions. With increasing reaction time, the yield of acetic acid continuously increased, whereas the yield of formic acid dropped noticeably because it was over-oxidized to CO_2. Methanol is similarly affected. However, acetic acid is more difficult to oxidize than the other liquid oxygenates, in agreement with the effect of oxygen shown in Fig. 1. After 2 h, the selectivity to liquid oxygenates dropped to 45% and CO_2 became the dominant oxidation product. The selectivity to acetic acid compared to the other liquid oxygenates was highest under these conditions (51%).

Extended Data Fig. 5a shows the UV–Vis absorption spectra of bare ZSM-5 (bottom trace), as-synthesized 0.5 wt% Rh-ZSM-5 (top trace), and 0.5 wt% Rh-ZSM-5 O_2 (middle trace). Compared to bare ZSM-5, as-synthesized 0.5 wt% Rh-ZSM-5 exhibits one additional absorption band centred at 265 nm. A similar absorption band has been observed in organometallic Rh(I) compounds and is assigned to the Rh^+ cations[33]. Therefore, we assigned this absorption band to isolated Rh^+ cations anchored on the internal walls of the zeolite. For 0.5 wt% Rh-ZSM-5 O_2, a much broader absorption band centred at 620 nm is present. The latter peak may be assigned to Rh(III)/Rh(IV) oxides[34]. Clearly, for 0.5 wt% Rh-ZSM-5 treated with H_2, UV–Vis absorption data show that a larger portion of Rh species are isolated Rh^+ cations, whereas for 0.5 wt% Rh-ZSM-5 calcined in static air, the majority of Rh species are Rh oxides.

Extended Data Fig. 5b shows the normalized XANES spectra of 0.5 wt% Rh-ZSM-5_{washed}, 0.5 wt% Rh-ZSM-5_{washed} suspended in water, 0.5 wt% Rh-ZSM-5_{washed} after reaction, as-synthesized 0.5 wt% Rh-ZSM-5, 0.5 wt% Rh-ZSM-5 O_2, as well as various Rh standards. XANES data of Rh-ZSM-5 were collected at room temperature in fluorescence mode. For 0.5 wt% Rh-ZSM-5_{washed} suspended in water, the measurement was performed in aqueous conditions after dispersing the catalyst powder in deionized water at room temperature. Approximately five consecutive scans were collected for each sample to improve the signal-to-noise ratio. Four standard samples, Rh_2O_3, $Rh(II)_2(CH_3COO)_4$, $Rh(I)_2(\mu\text{-}OH)_2(C_8H_{12})_2$ and Rh foil, were used as reference samples. The XANES data of the standards were collected in the transmission mode at room temperature. The absorption edge of 0.5 wt% Rh-ZSM-5_{washed} clearly shows that Rh species in Rh-ZSM-5 are not metallic but are in the cationic state. Linear combination fitting was performed and found no metallic Rh, only cationic Rh in the +1 oxidation state. The linear combination fitting of 0.5 wt% Rh-ZSM-5_{washed} after reaction shows 80% Rh^+ and 20% metallic Rh. For as-synthesized 0.5 wt% Rh-ZSM-5, the fitting shows that it consists of 60% Rh^+ and 40% metallic Rh, whereas for 0.5 wt% Rh-ZSM-5 O_2, Rh is in the +3 oxidation state. Moreover, XANES spectra collected with the catalyst sample suspended in water are similar to those for the sample in the absence of water.

Extended Data Fig. 6 shows the Rh K-edge EXAFS data of 0.5 wt% Rh-ZSM-5_{washed}, 0.5 wt% Rh-ZSM-5_{washed} suspended in water, and Rh foil. EXAFS data of Rh-ZSM-5 were collected at room temperature in fluorescence mode. EXAFS data of Rh-ZSM-5 suspended in water were collected at room temperature in fluorescence mode after dispersing the zeolite powder in water. EXAFS data of Rh foil were collected at room temperature in the transmission mode. Five consecutive scans were collected for each sample to improve the signal-to-noise ratio. The quantitative analyses for Rh–O and Rh–Rh contributions are shown in Extended Data Table 2. The analyses reveal that there is no distinct Rh–Rh bonding in 0.5 wt% Rh-ZSM-5_{washed}, indicating the presence of isolated Rh cations on the micropore walls of the zeolite. Moreover, the relatively short Rh–O bond length in Rh-ZSM-5, 1.99 ± 0.03 Å (compared to a Rh–O bond length of 2.70 Å in zeolite-supported Rh nanoclusters[35]) confirms that the Rh–O bonds in Rh-ZSM-5 are not attributed to zeolite-supported Rh nanoclusters. This bond length is also comparable to the Rh–O bond length observed in isolated Rh complexes anchored

on HY zeolite[36]. EXAFS measurements performed in the presence of water also show that water does not affect the isolation properties of Rh cations.

Extended Data Fig. 7 shows the possible reaction pathway of oxidative methane conversion to methanol and acetic acid on Rh-ZSM-5. In the first step, CH_4 can be activated on the mononuclear Rh^+ cation in the presence of O_2 and water to form Rh–CH_3 species. The formed Rh–CH_3 species can be further functionalized either through an oxygen-insertion reaction to form Rh–OCH_3 or a carbonylation CO-insertion reaction to form Rh–$COCH_3$. Subsequent hydrolysis of Rh–OCH_3 and Rh–$COCH_3$ gives methanol and acetic acid as products, respectively, and regenerates the Rh^+ catalyst, which closes the catalytic cycle.

Extended Data Fig. 8a shows the Rh K-edge EXAFS spectra and fitting of the as-synthesized 0.5 wt% Rh-ZSM-5 catalyst without washing. EXAFS spectra clearly show Rh–Rh bonding, indicating the presence of Rh nanoparticles in the as-synthesized 0.5 wt% Rh-ZSM-5 catalyst without washing. The Rh K-edge EXAFS spectra and fitting of 1.0 wt% Rh-ZSM-5_{washed} are shown in Extended Data Fig. 8b. The presence of Rh nanoparticles in 1.0 wt% Rh-ZSM-5_{washed} is obvious in the EXAFS spectra. Furthermore, Extended Data Fig. 8c shows Rh K-edge EXAFS spectra and fitting of the used 0.5 wt% Rh-ZSM-5_{washed} catalyst. The sample was obtained after methane conversion reaction using the 0.5 wt% Rh-ZSM-5_{washed} sample at 20 bar CH_4, 5 bar CO, 2 bar O_2 and 150 °C for 3 h. The EXAFS spectra show Rh–Rh bonding (coordination number = 0.6 ± 0.2), indicating the formation of some Rh clusters during the methane conversion reaction. Quantitative analyses for the Rh–O and Rh–Rh contributions in Extended Data Fig. 8 are shown in Extended Data Table 2.

The possibility of homogeneous reaction was investigated on Rh-ZSM-5 catalysts. After a 1-h reaction using 0.5 wt% Rh-ZSM-5, the zeolite particles were removed by centrifugation and an additional 1-h reaction was run under the same conditions using the collected reaction liquid. We did not observe any increase in liquid oxygenates after the additional 1-h test. Although after longer reaction times ($t = 12$ h) there was a trace amount of Rh in the water after the reaction, attributed to the dissolution of the few rhodium nanoparticles present on the external surface of the zeolite particles, our testing also found that such small amounts of Rh species in the water are not active. We conclude that the catalytic reaction under the conditions reported here is heterogeneous.

The Rh-ZSM-5 catalyst was inactive in solvents other than water, for example in ethylene glycol. Furthermore, using alkaline (pH = 10) or acidic media (pH = 2) rather than water did not have any beneficial effect on the catalytic performance. Therefore, water either promotes or directly acts as a co-catalyst in the oxidative conversion of methane to methanol and acetic acid.

In the case of Rh–Na-ZSM-5 (Fig. 1d), adding copper(II) nitrate (molar ratio Rh:Cu = 1:2) into the suspension suppresses the formation of formic acid. A similar effect has been reported before, and was attributed to the prevention of the over-oxidation of products to formic acid[1]. It is likely that the presence of Cu cations in our system play the same role, suppressing the formation of formic acid under our reaction conditions.

One may expect that the concentration of methane, oxygen and carbon monoxide in the micropores of ZSM-5 will be affected by limited solubility. However, several recent studies have reported that the solubility of gas molecules in water confined in the micropores or mesopores of zeolites, as compared to the bulk solubility, can be largely enhanced[3,37]. For example, it has been reported that the solubility of methane, nitrogen and carbon dioxide is as much as thirty times greater in the micropores of ZSM-5 compared with their bulk solubility[37]. Moreover, our data show that the reaction is catalytic, indicating the continuous presence of these gases in the micropores of the zeolite. Therefore, the concentration of these gases in the pores of ZSM-5 is sufficiently high for the catalytic reaction to proceed.

The stability of the Rh active species was evaluated under our reaction conditions. After a 3-h reaction using as-synthesized 0.5 wt% Rh-ZSM-5 at 20 bar CH_4, 5 bar CO, 2 bar O_2 and 150 °C, we filtered and collected the catalyst for a second cycle test. The second 3-h test using identical operating conditions to the first produced lower (by 25%) yields of oxygenates, but similar selectivities, with the loss probably owing to Rh atom diffusion and aggregation. Indeed, Rh nanoclusters were formed in the used 0.5 wt% Rh-ZSM-5_{washed} catalyst as shown by EXAFS in Extended Data Fig. 8c, whereas the fresh catalyst mostly comprised mononuclear Rh species. Preventing the sintering of isolated Rh atoms by proper tuning of the operating conditions to improve the stability of the Rh-ZSM-5 catalyst, or finding a way to regenerate the catalyst, is a key objective for future applications of this type of catalyst.

The alternative explanation of stability loss due to metal leaching is not relevant to our catalyst and reaction conditions. Rh leaching from 0.5 wt% Rh-ZSM-5 was checked by ICP–OES analysis of the reaction liquid at different reaction times. Aqueous-phase Rh was not detected throughout the course of reaction for the conditions in Fig. 1a. Similarly, no Rh leaching was detected for 0.6 wt% Rh/TiO_2 catalyst. Furthermore, as shown in Extended Data Fig. 1, the zeolite structure remains intact after reaction and no desilication or dealumination was observed by ICP analysis. Only after longer reaction times ($t = 12$ h) was there a trace amount of Rh in the water after the reaction, attributed to the leaching of the few rhodium nanoparticles on the external surface of the zeolite particles, as mentioned previously. Notably, our washing experiments also found that it is extremely difficult to remove anchored Rh species from the zeolite support after the hydrogen reduction step. It has been reported that metal cations anchored in the micropores of ZSM-5 are very stable against leaching, thus leaching of rhodium cations is not expected under our mild reaction conditions[38,39]. Even under extremely harsh hydrothermal conditions, with high pressures of between 140 and 150 bar at 350 °C, the majority of anchored cations cannot be leached out[40].

To identify the carbon source in the oxygenates, isotope-labelled ^{13}CO was used under typical reaction conditions using 0.5 wt% Rh-ZSM-5 and 0.6 wt% Rh/TiO_2. ^1H NMR confirms the formation of liquid oxygenates, which were further analysed by ^{13}C NMR. For 0.5 wt% Rh-ZSM-5, formic acid, methanol and acetic acid are the liquid products. Among them, $CH_3{}^{13}COOH$ is the only labelled liquid oxygenate present. No formation of $^{13}CH_3OH$, $^{13}CH_3COOH$ or $H^{13}COOH$ was identified. For Rh/TiO_2, methanol is the only liquid oxygenate, and no labelled $^{13}CH_3OH$ could be detected using ^{13}C NMR. These measurements confirm that the methyl group carbon is derived solely from methane, not from carbon monoxide, whereas acetic acid is formed through carbonylation insertion of CO.

Data availability. The main data supporting the findings of this study are available within the article and its Extended Data. Extra data are available from the corresponding author upon request.

28. Yang, M., Allard, L. F. & Flytzani-Stephanopoulos, M. Atomically dispersed Au–$(OH)_x$ species bound on titania catalyze the low-temperature water-gas shift reaction. *J. Am. Chem. Soc.* **135,** 3768–3771 (2013).
29. Zapata, P. A., Faria, J., Ruiz, M. P., Jentoft, R. E. & Resasco, D. E. Hydrophobic zeolites for biofuel upgrading reactions at the liquid–liquid interface in water/oil emulsions. *J. Am. Chem. Soc.* **134,** 8570–8578 (2012).
30. Ravenelle, R. M. *et al.* Stability of zeolites in hot liquid water. *J. Phys. Chem. C* **114,** 19582–19595 (2010).
31. Su, J. *et al.* Highly sensitive methane catalytic combustion micro-sensor based on mesoporous structure and nano-catalyst. *Nanoscale* **5,** 9720–9725 (2013).
32. Zhu, Y. *et al. In situ* surface chemistries and catalytic performances of ceria doped with palladium, platinum, and rhodium in methane partial oxidation for the production of syngas. *ACS Catal.* **3,** 2627–2639 (2013).
33. Mavila, S., Rozenberg, I. & Lemcoff, N. G. A general approach to mono- and bimetallic organometallic nanoparticles. *Chem. Sci.* **5,** 4196–4203 (2014).
34. Lee, W.-T. *Tris(guanidinato)complexes of iridium and rhodium in the oxidation states +III and +IV: synthesis, characterization, and reactivity*. PhD thesis, Univ. of Iowa, http://ir.uiowa.edu/etd/2736/ (2011).
35. Lepage, M. *et al.* Promotion effects in the oxidation of CO over zeolite-supported Rh nanoparticles. *J. Phys. Chem. C* **112,** 9394–9404 (2008).
36. Martinez-Macias, C., Serna, P. & Gates, B. C. Isostructural zeolite-supported rhodium and iridium complexes: tuning catalytic activity and selectivity by ligand modification. *ACS Catal.* **5,** 5647–5656 (2015).
37. Ho, L. N., Schuurman, Y., Farrusseng, D. & Coasne, B. Solubility of gases in water confined in nanoporous materials: ZSM-5, MCM-41, and MIL-100. *J. Phys. Chem. C* **119,** 21547–21554 (2015).
38. Fu, W. *et al.* High activity and stability in the cross-coupling of aryl halides with disulfides over Cu-doped hierarchically porous zeolite ZSM-5. *Chem. Commun.* **51,** 5890–5893 (2015).
39. Wang, L. *et al.* Mesoporous ZSM-5 zeolite-supported Ru nanoparticles as highly efficient catalysts for upgrading phenolic biomolecules. *ACS Catal.* **5,** 2727–2734 (2015).
40. Robin, T. F., Ross, A. B., Lea-Langton, A. R. & Jones, J. M. Stability and activity of doped transition metal zeolites in the hydrothermal processing. *Front. Energy Res.* **3,** 51 (2015).

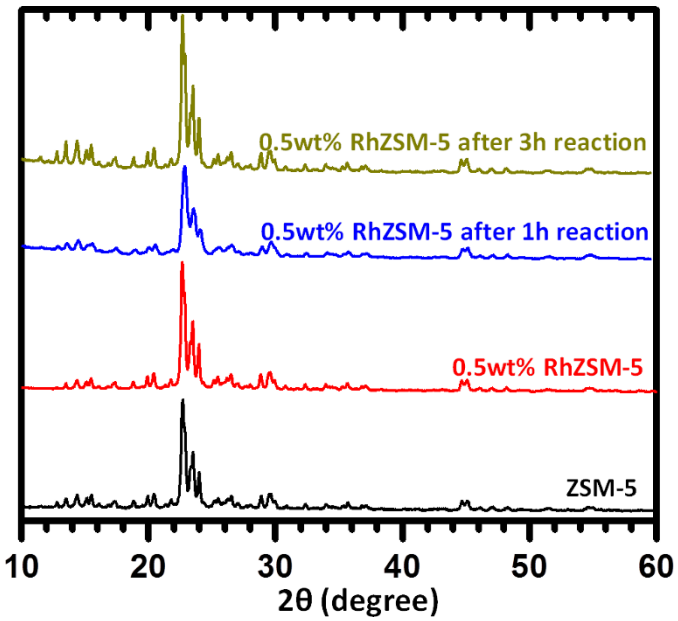

Extended Data Figure 1 | XRD patterns of bare ZSM-5, as-synthesized 0.5 wt% Rh-ZSM-5 and 0.5 wt% Rh-ZSM-5 after 1 h and after 3 h of reaction at 150 °C. XRD patterns of as-synthesized Rh-ZSM-5 show no observable difference compared with pure ZSM-5, indicating that the impregnation of Rh does not change the lattice structure of ZSM-5. The XRD patterns of Rh-ZSM-5 catalysts after the 1-h reaction and the 3-h reaction are preserved, suggesting that the oxidative conversion of methane to liquid oxygenate products does not alter the lattice structure of ZSM-5.

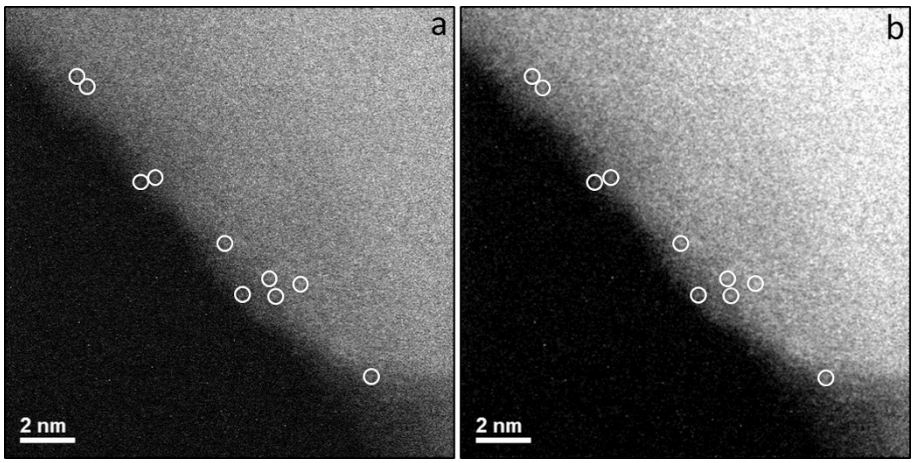

Extended Data Figure 2 | Aberration-corrected HAADF/STEM images of as-synthesized Rh-ZSM-5. a, Raw HAADF/STEM image. **b**, HAADF/STEM image after five-point smoothing and small contrast enhancement (Fig. 2a in main text). The images are of a thin edge of the as-synthesized Rh-ZSM-5 flake, where it is possible to image the Rh atoms. Contrast points consistent with the imaging of single Rh atoms are circled.

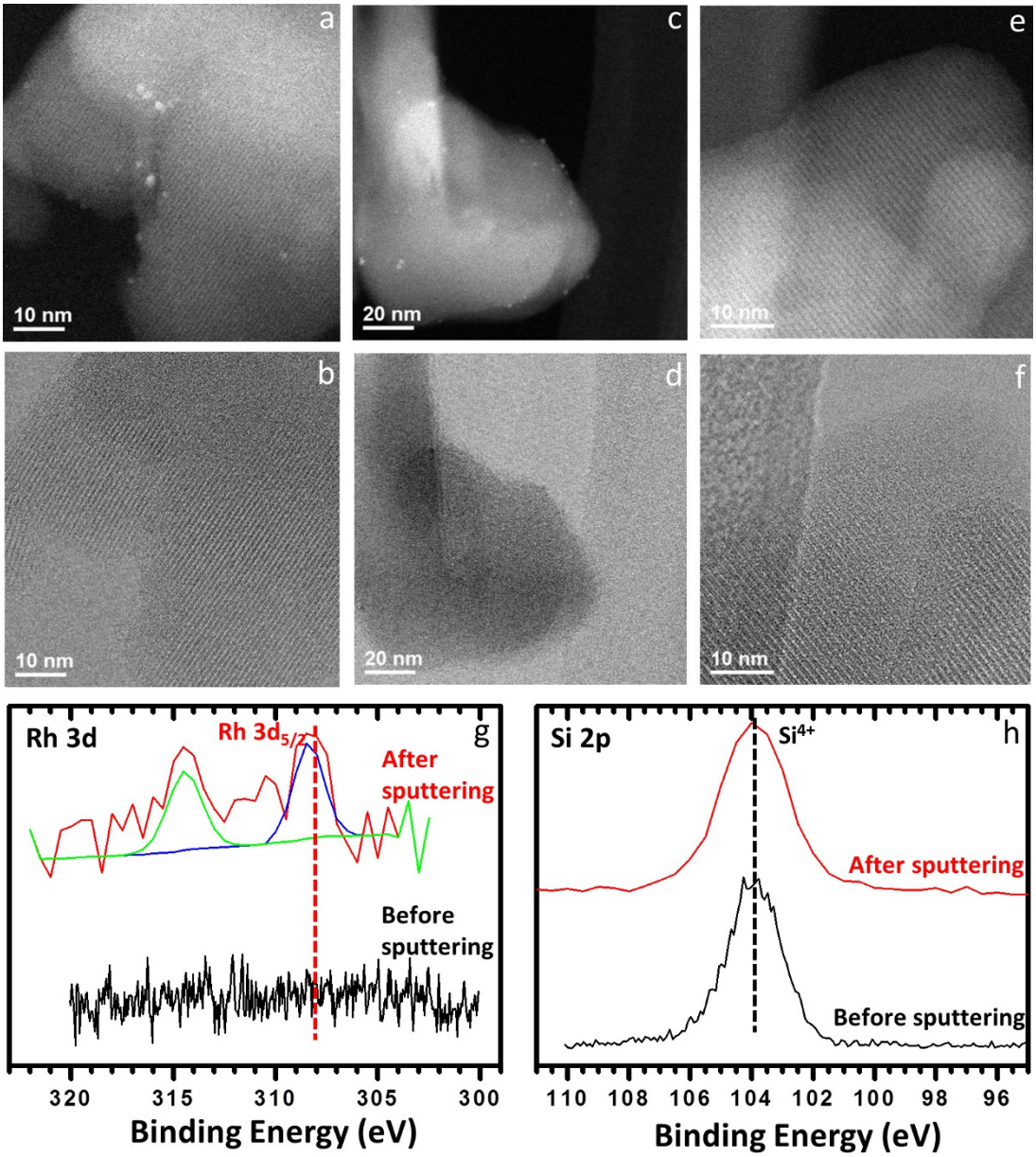

Extended Data Figure 3 | TEM images and XPS characterization of Rh-ZSM-5. a, **b**, Ac-HAADF (**a**) and bright-field (**b**) image pairs, acquired simultaneously, of as-synthesized 0.5 wt% Rh-ZSM-5. **c**, **d**, Ac-HAADF (**c**) and bright-field (**d**) image pairs of 0.5 wt% Rh-ZSM-5 after use in the reaction. **e**, **f**, Ac-HAADF (**e**) and bright-field (**f**) image pairs of 0.5 wt% Rh-ZSM-5_{washed}. The ac-HAADF images show that there are a few Rh nanoparticles on the external surface of zeolite for the samples without washing, whereas for the sample of Rh-ZSM-5_{washed} there are no Rh nanoparticles present. **g**, The Rh 3*d* photoemission spectra of as-synthesized 0.5 wt% Rh-ZSM-5 before and after Ar^+ ion sputtering. **h**, The Si 2*p* photoemission spectra of as-synthesized 0.5 wt% Rh-ZSM-5 before and after Ar^+ ion sputtering. Before sputtering, no photoemission peak of Rh was observed on Rh-ZSM-5. After Ar^+ ion sputtering for 5 min, a Rh 3*d* feature arising from the Rh species anchored on the internal walls of the zeolite was clearly identified. XPS characterization therefore confirms the presence of Rh species inside the micropores of the zeolite.

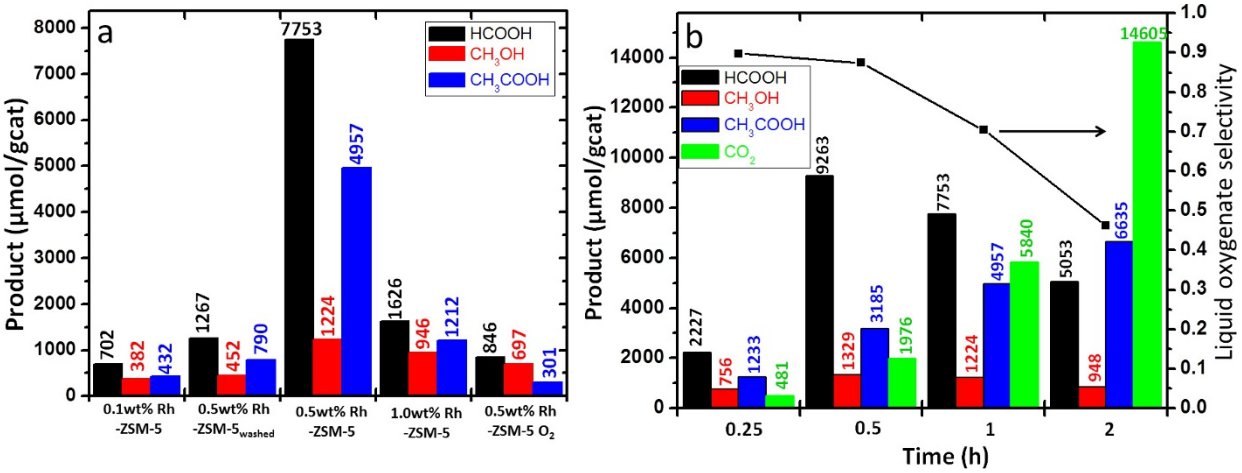

Extended Data Figure 4 | Catalytic performance of various Rh-ZSM-5 catalysts in the direct conversion of methane to liquid oxygenates. **a**, Yields of liquid oxygenates on Rh-ZSM-5 catalysts with different Rh loadings, as well as 0.5 wt% Rh-ZSM-5_{washed} and 0.5 wt% Rh-ZSM-5 O_2. Reaction conditions: 20 mg catalyst, 20 bar CH_4, 5 bar CO, 4 bar O_2, 150 °C, 1 h. **b**, Product yields and liquid oxygenate selectivity at various reaction times with a p_{O_2} of 4 bar, using the as-synthesized 0.5 wt% Rh-ZSM-5 catalyst. Reaction conditions: 20 mg catalyst, 20 bar CH_4, 5 bar CO, 4 bar O_2, 150 °C, and various reaction times. All data points were replicated three times and average values are reported with uncertainty below 10%.

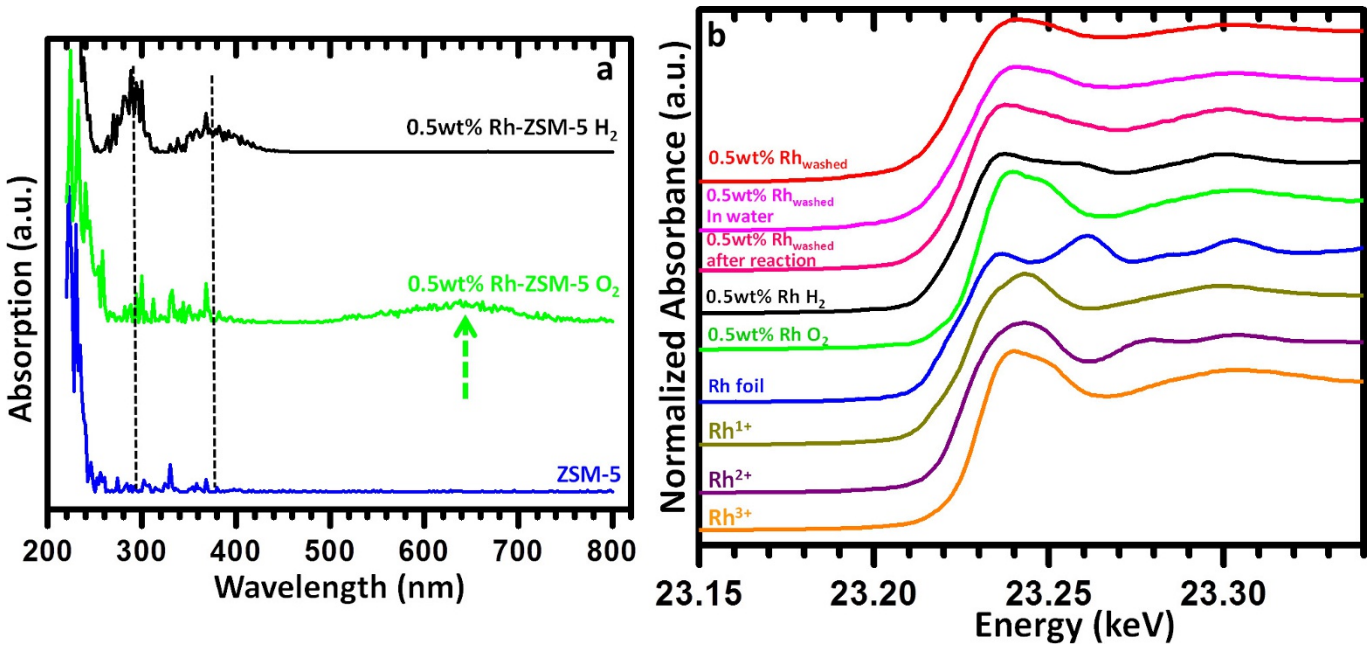

Extended Data Figure 5 | UV–Vis absorption spectra and XANES spectra of various samples. a, UV–Vis absorption spectra of bare ZSM-5 (bottom trace), as-synthesized 0.5 wt% Rh-ZSM-5 (top trace), and 0.5 wt% Rh-ZSM-5 O_2 (middle trace). **b**, Normalized XANES spectra of 0.5 wt% Rh-ZSM-5_{washed}, 0.5 wt% Rh-ZSM-5_{washed} suspended in water, 0.5 wt% Rh-ZSM-5_{washed} after reaction, as-synthesized 0.5 wt% Rh-ZSM-5, 0.5 wt% Rh-ZSM-5 O_2, as well as various Rh standards (Rh^+: [Rh(μ-OH)(COD)]$_2$, Rh^{2+}: [$Rh(CH_3COO)_2$]$_2$, Rh^{3+}: Rh_2O_3).

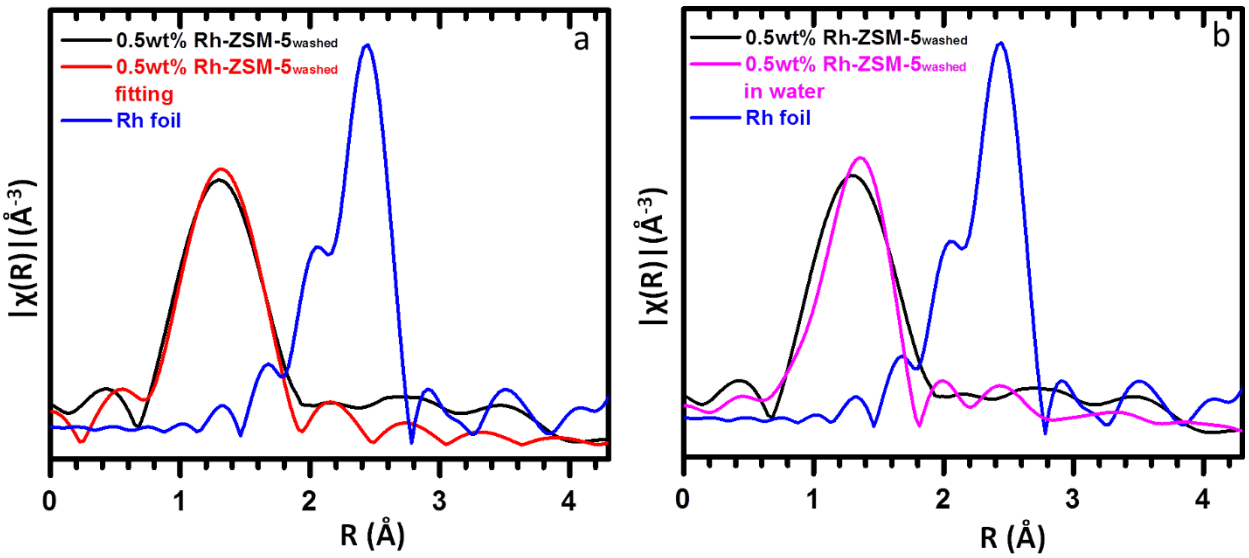

Extended Data Figure 6 | EXAFS characterization of 0.5 wt% Rh-ZSM-5$_{washed}$ samples under different conditions and Rh foil standard. a, Rh K-edge EXAFS spectra of 0.5 wt% Rh-ZSM-5$_{washed}$, Rh foil, and the fitting of 0.5 wt% Rh-ZSM-5$_{washed}$. **b**, Rh K-edge EXAFS spectra of 0.5 wt% Rh-ZSM-5$_{washed}$, 0.5 wt% Rh-ZSM-5$_{washed}$ suspended in water, and Rh foil. EXAFS spectra of the Rh-ZSM-5 sample were collected at room temperature in fluorescence mode. EXAFS spectra of Rh foil were collected at room temperature in the transmission mode. Note that in these cases, radial distances are given without phase correction. Quantitative analyses of Rh–O and Rh–Rh contributions in 0.5 wt% Rh-ZSM-5$_{washed}$ are shown in Extended Data Table 2, Entry 1.

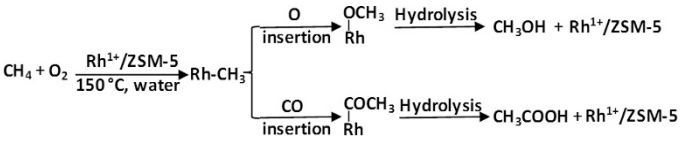

Extended Data Figure 7 | Possible reaction pathways of the catalytic conversion of methane to methanol and acetic acid on Rh-ZSM-5. The conversion to methanol and acetic acid follow independent reaction pathways. See the main text for more information.

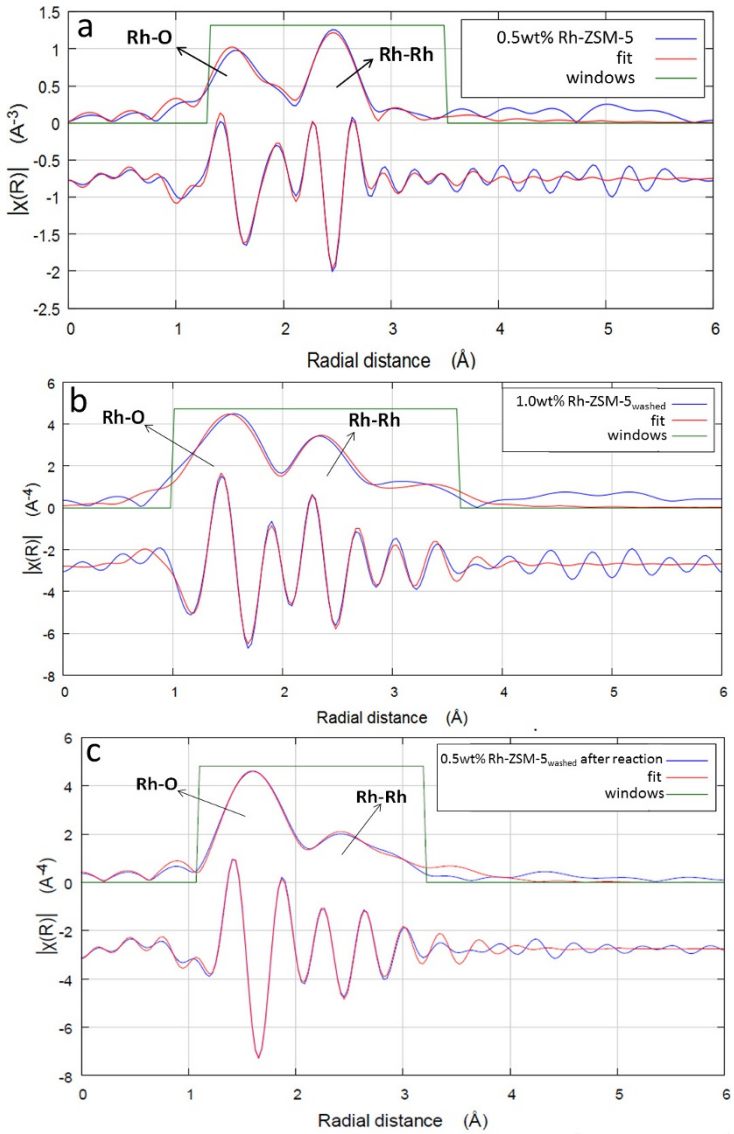

Extended Data Figure 8 | EXAFS characterization of various Rh-ZSM-5 catalysts. a, Rh K-edge EXAFS spectra and fitting of 0.5 wt% Rh-ZSM-5 without washing. EXAFS spectra clearly show Rh–Rh bonding, indicating the presence of Rh nanoparticles in the 0.5 wt% Rh-ZSM-5 sample without washing. **b**, Rh K-edge EXAFS spectra and fitting of 1.0 wt% Rh-ZSM-5_{washed}. EXAFS spectra clearly show Rh–Rh bonding, indicating the presence of Rh nanoparticles. **c**, Rh K-edge EXAFS spectra and fitting of used 0.5 wt% Rh-ZSM-5_{washed} catalyst. The sample was obtained after methane conversion reaction using the 0.5 wt% Rh-ZSM-5_{washed} catalyst at 20 bar CH_4, 5 bar CO, 2 bar O_2 and 150 °C for 3 h. EXAFS spectra clearly show Rh–Rh bonding, indicating the formation of Rh clusters during the methane conversion reaction. The quantitative analyses for Rh–O and Rh–Rh contributions in these samples are shown in Extended Data Table 2.

Extended Data Table 1 | Calculated conversion of methane at different reaction times

Reaction time (h)[#]	1	2	3	6
Total amount of products (μmol)[+]	54	65	168	475
Calculated CH_4 conversion (%)*	0.4	0.5	1.4	4.0

Data from Fig. 1b. #Reaction conditions: 20 mg catalyst, 2 bar O_2, 5 bar CO, 20 bar CH_4, 20 ml water, 150 °C. [+]The products are: HCOOH, CH_3OH, CH_3COOH, and CO_2. *The amount of CH_4 charged into the reactor is calculated from 20 bar of CH_4 at RT. The volume of gas is 15 ml, which corresponds to 12 mmol CH_4.

Extended Data Table 2 | Quantitative analyses of Rh–O and Rh–Rh contributions as measured by EXAFS

Sample	Shell	CN[(a)]	$R(\text{Å})^{(b)}$	$\sigma^2(\text{Å}^2)$	EXAFS Fitting Plot
0.5wt% Rh-ZSM-5$_{washed}$	Rh-O	3.6 ± 0.6	1.99 ± 0.03	0.007	Extended Data Fig. 6a
	Rh-Rh	0			
0.5wt% Rh-ZSM-5	Rh-O	3.0 ± 0.7	2.03 ± 0.04	0.005	Extended Data Fig. 8a
	Rh-Rh	5.7 ± 1.1	2.69 ± 0.03	0.015	
1.0wt% Rh-ZSM-5$_{washed}$	Rh-O	3.1 ± 0.5	2.02 ± 0.02	0.003	Extended Data Fig. 8b
	Rh-Rh	1.7 ± 0.2	2.68 ± 0.02	0.012	
0.5wt% Rh-ZSM-5$_{washed}$ after reaction	Rh-O	2.7 ± 0.6	2.03 ± 0.02	0.003	Extended Data Fig. 8c
	Rh-Rh	0.6 ± 0.2	2.70 ± 0.01	0.005	

Data from Extended Data Figs 6 and 8. a, CN, coordination number; b, *R*, distance between absorber and backscattered atoms.